2014

Analysis of vesicular porosity in soils using high-resolution X-ray computed tomograpy

Judith K. Turk
Richard Stockton College of New Jersey, jturk3@unl.edu

Robert C. Graham
University of California, Riverside, robert.graham@ucr.edu

Published August 25, 2014

Analysis of Vesicular Porosity in Soils using High Resolution X-Ray Computed Tomography

Judith K. Turk*
Environmental Sciences Program
Richard Stockton College of New Jersey
Galloway, NJ 08205

Robert C. Graham
Soil and Water Sciences Program
Dep. of Environmental Sciences
Univ. of California
Riverside, CA 92521

Vesicular horizons are common at the surface of arid and semiarid soils and play a critical role in regulating infiltration. Most methods for examining pore morphology in the vesicular horizon involve physical sectioning of the sample and individual measurement of pores, which is time-consuming and provides an incomplete view of the pores. The objectives of this study were to (i) develop methods for the classification and characterization of pores in the vesicular horizon using high resolution X-ray computed tomography (HRXCT) and (ii) use these methods to examine the distribution of pores within vesicular peds. Three intact peds were scanned by HRXCT and examined using Blob3D software. A subset of pores from the first scan were observed and used to develop a classification tree model based on quantitative parameters of pore shape. Five major pore classes were found: equant vesicles, nonequant vesicles, individual vughs, connected vughs, and planar voids. All pore types decreased in size with increasing depth in the samples; however, the trend in quantity of pores with depth varied between pore types. In the ped with the least vesicular porosity, there was an increase in size and decrease in number of all pore types between the ped interior and exterior, a pattern which was reduced in the peds that were more dominantly vesicular. The application of HRXCT in this study shows how pore shape and size can be quantified within the vesicular horizon and reveals considerable variation of these characteristics within and between peds.

Abbreviations: AR1, aspect ratio 1 (longest/shortest axis); AR2, aspect ratio 2 (longest/second-longest axis); HRXCT, high resolution X-ray computed tomography; SNSVR, sphere-normalized surface to volume ratio; VHI, vesicular horizon index.

Vesicular horizons are a widely occurring feature of soils in arid and semiarid lands, with critical implications for the surface hydrology of water-limited ecosystems. Vesicular horizons occur at or near the soil surface and are characterized by the predominance of discontinuous, nearly spherical vesicular pores. They have been observed on every continent on Earth and cover large areas of land in arid and semiarid regions (Ellis, 1990; Turk and Graham, 2011) but are generally limited to regions receiving <350 mm of mean annual precipitation (Dietze et al., 2012). The vesicular horizon often occurs beneath a surficial monolayer of embedded gravels known as reg (Dan et al., 1982; Amit and Gerson, 1986) or desert pavement (Clements et al., 1957; Musick, 1975). The entrapment of dust beneath the desert pavement lifts the gravels at the surface and creates an eolian layer that often develops vesicular porosity (McFadden et al., 1987; Wells et al., 1995; Wood et al., 2005; Valentine and Harrington, 2006; Ugolini et al., 2008). The texture of this horizon is most often in the loam, silt loam, or sandy loam textural classes (Turk and Graham, 2011). In the Mojave Desert, periods of high eolian activity, caused by the drying of pluvial lakes during the Pleistocene-to-

Soil Sci. Soc. Am. J. 78:868–880
doi:10.2136/sssaj2013.12.0541
Received 22 Dec. 2013.
*Corresponding author (judith.turk@stockton.edu).

Holocene transition period, have been hypothesized as a cause of widespread dust accretion and vesicular horizon formation (McFadden et al., 1998; Anderson et al., 2002).

Within the desert landscape, vesicular horizons display fine-scale heterogeneity. They occur extensively in the intercanopy soils between shrubs but are absent or weakly expressed beneath the shrub canopy (Wood et al., 1978; Shafer et al., 2007). The absence of vesicular porosity beneath the shrub canopy has been attributed to factors such as the dissipation of raindrop energy, which prevents surface crusting (Hillel, 1998) and the disruption of the surface by root channels and rodent burrows, which become dominate transport pathways for water and air (Dietze et al., 2012). Variability of surface properties in arid soils leads to heterogeneous infiltration rates, which control runoff and run-on patterns (Abrahams and Parsons, 1991). Soils with vesicular horizons have much lower infiltration rates compared to nonvesicular soils of shrub islands, ephemeral washes, and young alluvial deposits (Turk and Graham, 2011). Many studies have illustrated that the pore characteristics of the vesicular horizon are responsible for the reduced infiltration rates of the vesicular soils. Negative correlations have been observed between the amount of vesicular porosity in the surface horizon and infiltration rates (Blackburn, 1975; Valentin, 1994; Lebedeva et al., 2009), and infiltration rates have been shown to decrease when vesicular porosity is recreated by repeated wetting and drying of soil samples in the lab (Dietze et al., 2012). Thus, vesicular horizons favor runoff over leaching, which limits the plant water supply and leads to decreased leaching of salts and consequently increases plant osmotic stress due to high soil salinity (Musick, 1975; Wood et al., 2005). With increasing soil development, vegetation becomes more restricted to shrub islands and ephemeral washes, where run-on accumulates (Noy-Meir, 1973; Musick, 1975; McAuliffe, 1994).

Vesicular horizons are usually 1 to 10 cm thick (Wood et al., 1978; Dan et al., 1982; Ugolini et al., 2008; Yonovitz and Drohan, 2009; Turk and Graham, 2011; Dietze et al., 2012). The vesicular pores range from less than one to a few mm in diameter (Anderson et al., 2002; Dietze et al., 2012) and can be equant, oblate, or prolate in shape with smooth walls (Brewer, 1976; Sullivan and Koppi, 1991; Stoops, 2003). In addition to the rounded vesicular pores, irregular pores are also often observed in the vesicular soil horizon. These pores have been referred to as vughs by some authors (Figueira and Stoops, 1983; Yonovitz and Drohan, 2009) or included as vesicles by others (Dietze et al., 2012). Vughs have been considered to form by the coalescence of vesicles (Dietze et al., 2012) and are sometimes connected by narrow channels (Brewer, 1976; Sullivan and Koppi, 1991; Dietze et al., 2012). Vesicular horizons may be massive or platy, but in their more developed form they have a primary structure consisting of columns or prisms that part to a secondary platy structure (McFadden et al., 1998; Anderson et al., 2002; Dietze et al., 2012).

Vesicular pores are formed by the entrapment of air in soil during wetting events (Hugie and Passey, 1964; Miller, 1971; Figueira and Stoops, 1983; Stoops, 2003). Bubbles can be observed rising through the vesicular horizon when it is in the fluid, supersaturated condition (Hugie and Passey, 1964). As the soil dries and hardens, the bubbles get trapped, forming vesicular pores. Vesicular horizons occur in association with "sealed" surfaces, which many authors have suggested to play a critical role in the formation of the vesicular pores, although the exact mechanism is debated. Various authors have suggested that the seal impedes the escape of entrapped air (Evenari et al., 1974; Ellis, 1990). Others have suggested that negative pressure is created by a wetting front advancing beneath a surface seal, leading to the effervescence of dissolved gases (Hillel, 1998; Dietze et al., 2012). Surfaces that produce an effective seal include embedded gravels (Evenari et al., 1974; Figueira and Stoops, 1983; Valentin, 1994), physical crusts (Hugie and Passey, 1964; Miller, 1971; Brewer, 1976; Evenari et al., 1974; Hillel, 1998; Cantón et al., 2003; Badorreck et al., 2013), and biological soil crusts (Evenari et al., 1974; Malam Issa et al., 1999; Joeckel and Clement, 1999; Cantón et al., 2003; Williams et al., 2012). Gravels form an effective surface seal when they are embedded in the underlying sediment, but protect the surface from sealing and vesicle formation if they are nonembedded (Valentin, 1994). This explains why the embedded gravels of desert pavement and reg surfaces have such widespread association with vesicular soils horizons. Other hypothesized mechanisms of vesicular pore formation include production of biogenic gases by soil microorganisms (Paletskaya et al., 1958), CO_2 released as $CaCO_3$ precipitates during drying (Paletskaya et al., 1958; Evenari et al., 1974; Lebedeva et al., 2009), and thermal expansion of gases due to solar heating (Evenari et al., 1974; Henning and Kellner, 1994; Brown and Dunkerley, 1996). All three of these hypotheses have been shown to be of minor significance by experimental manipulation of samples used to recreate vesicular pores in the laboratory (Dietze et al., 2012; Turk, 2012).

There is a need for quantitative methods of analyzing and describing pores in the vesicular horizon to discern differences between vesicular horizons formed under different conditions or displaying different hydrologic behaviors (Dietze et al., 2012). A semi-quantitative characterization of vesicular porosity can be made in the field using the vesicular horizon index (VHI), which is based on horizon thickness and pore size and quantity classes assigned by visual assessment (Turk and Graham, 2011). Past studies of pore morphology in the vesicular horizon have used thin sections (Figueira and Stoops, 1983; Sullivan and Koppi, 1991; Yonovitz and Drohan, 2009) or photographs of a bisected ped taken under careful lighting conditions (Dietze et al., 2012). These studies have classified or described pores shapes using an index of roundness (Figueira and Stoops, 1983; Dietze et al., 2012), or the pore aspect ratio (Yonovitz and Drohan, 2009), and quantified the size of the pores in terms of their cross-sectional area exposed in the thin section.

In recent years, computed tomography has found many applications in the quantitative study of pore structure in soils and other porous media (Ketcham and Carlson, 2001; Brun et al.,

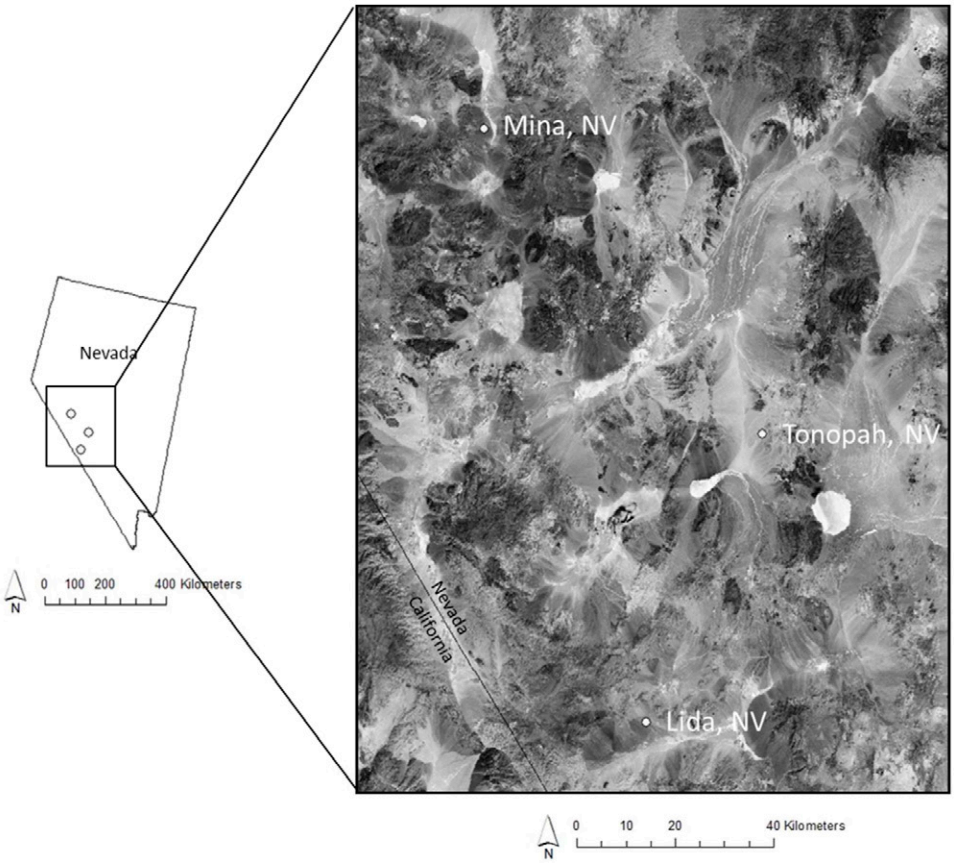

Fig. 1. Sampling location shown with respect to the Nevada state boundary and Landsat imagery (USGS, 2009).

2010). These methods offer more complete imagery of the pores in three dimensions and require no physical sectioning of the sample. We used HRXCT to characterize the pores of a vesicular horizon in three dimensions. The objectives of our study were to (i) develop methods for the classification and characterization of pores in the vesicular horizon using high HRXCT and (ii) use these methods to examine the intrapedal distribution of pores.

MATERIALS AND METHODS

Sample Collection

Three well-developed vesicular peds were collected from sites in the central Great Basin Desert. The sites were located in Nevada near the towns of Lida, Tonopah, and Mina (Fig. 1). Climate data from Tonopah, NV indicates a mean annual temperature of 11°C and mean annual precipitation of 150 mm for this region of the Great Basin. All sites were located on alluvial fan surfaces with desert pavement composed of mixed volcanic rock fragments and sparse vegetation composed of saltbush–greasewood scrub [*Sarcobatus vermiculatus* (Hook.) Torr., *Lycium shockleyi* A. Gray, *Ephedra nevadensis* S. Watson, and *Picrothamnus desertorum* Nutt.] (Table 1). Elevation of the sites ranged from 1429 to 1626 m. The soils at each of the sites were described and classified according to Soil Taxonomy (Soil Survey Staff, 2010). At Lida and Tonopah, the soils were Haplocambids and at Mina the soils were Haplargids. The alluvial fan surfaces are estimated to range in age from mid-Holocene to late Pleistocene based on interpretations of soil morphology in comparison to alluvial fan surfaces of known age in the region (Bell, 1995). The vesicular horizons at all three sites had moderate to strong columnar structure and loam textures. Vesicular horizon indexes range from 2.6 to 2.9, which is slightly greater than the median of 2.4 for the central Great Basin (Turk and Graham, 2011). The peds collected for analysis ranged in size from 4 to 4.5 cm in height and 7 to 8.5 cm in diameter (Fig. 2).

Computed Tomography Scanning and Segregation

The peds were scanned using HRXCT, with an interslice spacing of 0.08118 mm and a resolution of 0.0752 mm per pixel. The slices generated by the HRXCT scan were analyzed using the Blob3D software package (Ketcham, 2005). The Blob3D program has three main steps: segregation, separation, and extraction. In segregation, filters are applied to the greyscale images to define the content of each voxel (3D pixel). During separation, contiguous voxels of the same content type, called blobs, can be divided into sub-blobs, accepted as a whole, or rejected. Finally, the extraction step generates quantitative metrics of the separated blobs, such as surface area and volume.

Table 1. Sampling locations and soil characteristics.

Field site	Elevation, m	Landform†	Soil great group‡	VHI§	Estimate soil age¶	Vesicular horizon texture#
Lida, NV	1560	Inset fan	Haplocambids	2.6	Middle Holocene	loam
Tonopah, NV	1626	Erosional fan remnant	Haplocambids	2.7	Early Holocene	loam
Mina, NV	1429	Erosional fan remnant	Haplargids	2.9	Late Pleistocene	loam

† Determined by field observation and classified according to Peterson (1981).

‡ Determined by field observation and classified according to Soil Taxonomy (Soil Survey Staff, 2010).

§ Vesicular horizon index (Turk and Graham, 2011).

¶ Estimated from comparison to soil properties of data surfaces at the Mina, Nevada site (Bell, 1995).

Lab-determined textures by laser diffraction scanning (Eshel et al., 2004; Segal et al., 2009).

In this study, voids, gravels, and the scanned area outside of the sample were segregated for analysis, based on the greyscale values of TIFF images generated by the scan. The range of greyscale values for each segregation step was adjusted to find the best match between the selected pixels and our visual interpretation of voids and gravels. The scanned area outside of the sample was segregated with the voids and then distinguished as a different component during the separate step. All voids smaller than 0.065 mm^3 (corresponding to a 0.5-mm diam. sphere) were rejected due to difficulty resolving pores in this size range. Gravels were segregated using a 95% majority filter within a five-pixel radius, which improved detection of gravels by testing for homogeneity of the voxels. All gravel blobs <4.189 mm^3 were rejected because they are not large enough to be considered gravels.

Pore Classification

The pore classification scheme was developed using the sample from Lida, NV. This sample was selected as typical for the region because it has a VHI of 2.6, which is just slightly above the median for the central Great Basin (Turk and Graham, 2011). A cylindrical subvolume, consisting of the inner 3.5 cm and upper 2.6 cm of the sample, was selected for detailed analysis of the pore geometry. Every pore occurring entirely within the subvolume was examined, and the pore shape described. The total number of pores examined was 1130. The pores were described as they were segregated from the greyscale images by the Blob3D program without additional separations performed. For each pore, the sphere-normalized surface to volume ratio (SNSVR) was extracted. This value is equal to one for a perfect sphere and increases as the surface area increases above that expected for a sphere of a given volume (Jerram et al., 2009). Also, the lengths of the three axes defining the best fit ellipsoid were extracted for each pore and used to calculate two aspect ratios. The first aspect ratio (AR1) is the ratio of the longest to the shortest axis of the pore. The second aspect ratio (AR2) is the ratio of the longest to the second-longest axis of the pore. The extracted values (SNSVR, AR1, and AR2) and corresponding descriptions of pore shape were analyzed using the recursive partitioning package in R 2.15.0 (Hothorn et al., 2006) to develop a classification tree for the pores based on quantitative parameters. Of the 1130 pores analyzed, 799 (70%) were randomly selected to train the classification tree model, and the remaining 331 (30%) of the pores were used to test the agreement between the model-based classification and the pore shape described during observation.

Pore Characterization

Following development of the model-based classification system, the three complete samples were analyzed by extracting the model variables (SNSVR, AR1, and AR2) and classifying the pores according to the classification tree. Pore volume, gravel volume, maximum axis orientation, and *xyz* coordinates of the centroid of each pore were also extracted for analysis.

Using the extracted data, several terms were calculated to describe each pore type. The number of pores per gravel-free sample volume was used as a measure of pore quantity. Pore volumes were used as a measure of pore size and were log-normalized for all analyses. For pore classes defined by large aspect ratio, the maximum axis orientation relative to the x–y plane of the sample was also calculated by subtracting the orientation relative to the z plane from 90°.

Variability in pore class, quantity, and size within the peds was analyzed. For this analysis, the peds were divided two ways: vertically and horizontally. For the vertical division of the ped, pores were grouped by the z coordinate of the pore's centroid position into four groups: (i) 0 to 10 mm, (ii) 10 to 20 mm, (iii) 20 to 30 mm, and (iv) 30 to 40 mm. The volume of the sample within each depth range was determined to calculate the number of pores per gravel-free soil volume. This was accomplished by bringing only the slices corresponding to that depth range into Blob3D, segregating the empty volume surrounding the ped and

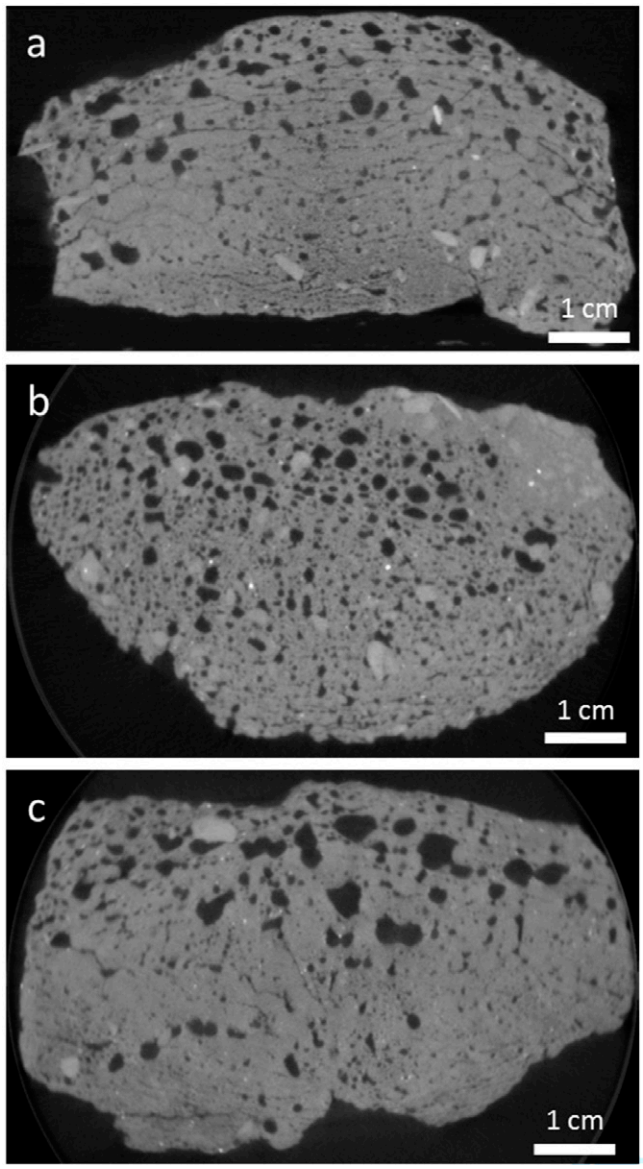

Fig. 2. A slice from the high resolution X-ray computed tomography scan of the vesicular peds from (a) Lida, NV, (b) Tonopah, NV, and (c) Mina, NV. Each slice is a vertical cross section through the ped, oriented so that the surface of the ped is at the top of the image.

the gravels within the ped, and finally subtracting these values from the total scanned volume within the depth range under consideration.

For the horizontal division of the peds, pores were grouped according to the distance of the pore's centroid position from the horizontal center of the ped, according the following equation:

$$\text{Distance from the horizontal center of the ped} = \sqrt{x^2 + y^2}$$

where x and y are the x and y coordinates of the pore's centroid position. The groups were (i) 0 to 10 mm, (ii) 10 to 20 mm, (iii) 20 to 30 mm, and (iv) 30 to 40 mm. The volume of each cylindrical ring-shaped subvolume, defined by each range of distances, was determined by cropping the scan slices at the inner and outer radius of each subvolume, bringing the cropped scans into Blob3D, and repeating the segregation of the empty volume surrounding the ped and the gravels within the ped. The outer-radius cylindrical volume was calculated, and the empty volume outside of the sample, gravel volume, and the inner-radius cylindrical volume were subtracted to determine the gravel-free sample volume of each cylindrical ring.

RESULTS AND DISCUSSION

Description of Pores

Observations using HRXCT imaging revealed that the vesicular horizon contains a variety pore types. Of the pores described in the sample from Lida, NV, 44% were some type of vesicular pore. The vesicular pores observed included equant, prolate, and oblate shapes (Fig. 3a, 3b, and 3c), which have been described previously in thin sections of vesicular horizons (Brewer, 1976; Sullivan and Koppi, 1991; Stoops, 2003). Another commonly observed vesicular pore shape was hemispherical (Fig. 3d), with the flattened side often bounded by the surface of a gravel or a planar void. Of the vesicles in the Lida sample, 35% were equant, 37% were oblate, 10% were prolate, and 18% were hemispherical, indicating that substantial diversity occurs, even in pores that can be classified as vesicles. Some channels connecting vesicular pores were observed but were not common enough to be quantified here.

The second class of pores observed in the sample was vughs (Fig. 4). These are large, irregular pore shapes that are not normally connected (Brewer, 1976, Stoops, 2003) and are often observed in the vesicular horizon (Figueira and Stoops, 1983; Yonovitz and Drohan, 2009). Vughs were nearly as common as vesicles, making up 40% of all pores described in the sample. Many mechanisms have been described to explain the formation of vughs, including flocculation of clay particles, welding of aggregates, differential mineral weathering, or faunal activity (Brewer, 1976; Stoops, 2003). However, the most likely mechanism of vugh formation in the vesicular horizon is the merging of adjacent vesicular pores as they grow (Dietze et al., 2012). This mechanism is supported by the vesicle-like lobes that make up many of the pores described here as vughs (Fig. 4a and 4b).

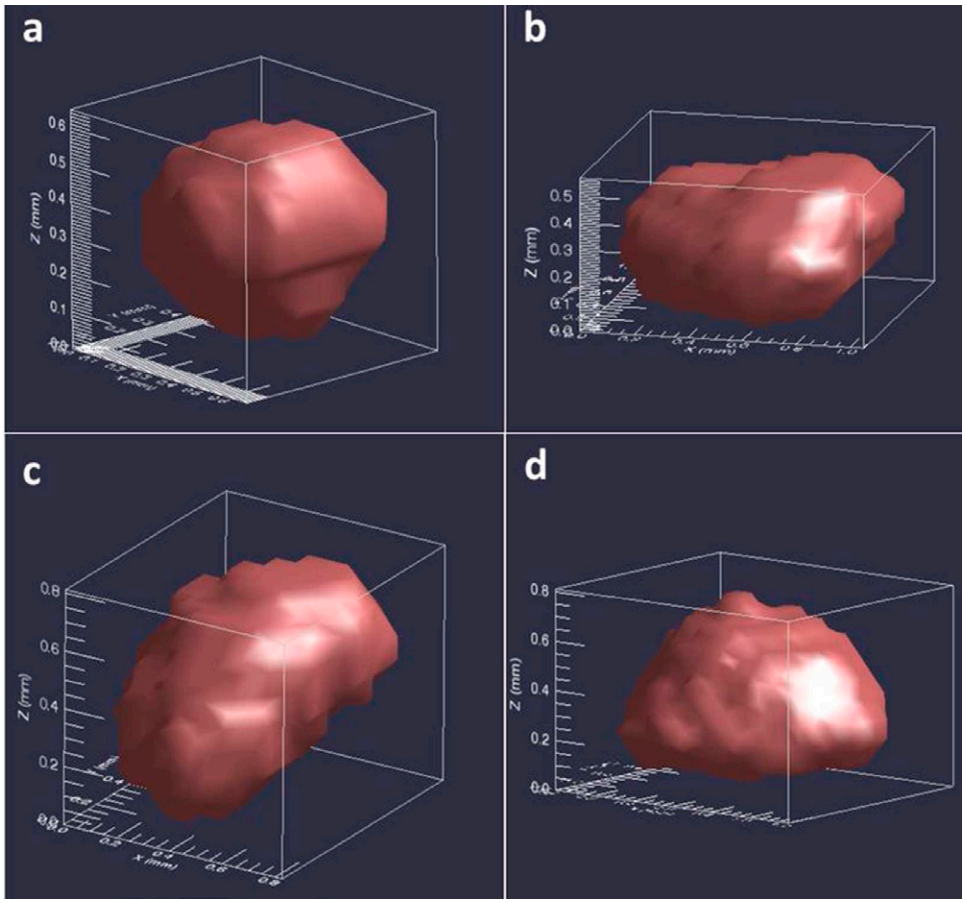

Fig. 3. Images of vesicular pores generated using Blob3D: (a) an equant vesicle, (b) an oblate vesicle, (c) a prolate vesicle, and (d) a hemispherical vesicle.

Vughs were sometimes interconnected by channels, forming either planar voids (Fig. 5a) or three-dimensional networks of pores (Fig. 4c and 4d). Such interconnected vughs have been described elsewhere (Brewer, 1976); however, previous quantitative examinations of porosity in the vesicular horizon have tended to overlook these interconnected networks. This may be due to the focus of previous studies on incipient vesicular porosity that has been recreated in the lab (Figueira and Stoops, 1983; Dietze et al., 2012) as well as the limitations of two-dimensional analysis in thin sections. By examining pores in

three-dimensions using HRXCT, all possible directions of interconnecting channels are included, which increases the likelihood of observing connections between the pores. However, even using HRXCT, the observation of small interconnecting channels is highly sensitive to the choice of greyscale range used to segregate voids. If too broad of a range is chosen, nonconnected pores may be interpreted as connected, while too narrow of a greyscale range will result in nondetection of small channels connecting pores. During the segregation stage of this study, neighboring pores that did not appear to be connected were observed and the greyscale range was expanded until the maximum limit at which the pores remained as discrete entities was reached. Thus, false connections between pores were avoided; however, the greyscale range may be too narrow to observe some interconnecting pores.

The final group of pores considered here are voids elongated along a single plane, which made up 17% of all pores described. These pores took a variety of forms. First, there were the vughs that were interconnected along a plane (Fig. 5a). Other planar voids included pores that were extremely flat and small in volume (Fig. 5b, 5c, and 5d). Such voids segregated from the HRXCT scan were often observed to be fragments of more extensive planar voids, which tapered into a zone that was too narrow to be segregated at the resolution of the scan. In some cases, channels connecting neighboring flattened pores were observable (Fig. 5b). Such planar voids are considered to correspond with the planes of weakness between platy aggregates that make up the vesicular horizon, such as those visible near the surface of the sample in Fig. 2a.

Based on these observations, and those of other researchers, a genetic pathway of pore development in the vesicular horizon may be outlined (Fig. 6). The first stage of pore development is the formation of equant vesicles, with a spherical shape that develops to reduce the air–water interface of air trapped in the soil (Miller, 1971). In the second stage, the equant vesicular shape is modified by compressional forces and the merging of vesicles. Equant vesicles may be compressed along one or more axes to form oblate, prolate, or hemispherical vesicles. In addition, as vesicular pores merge they form irregular shapes, described as vughs. Vughs, and some vesicles, become interconnected by narrow channels, possibly through the shrinkage of the intervening matrix during desiccation (Sullivan and Koppi, 1991). Formation of connecting channels along multiple axes results in a three-dimensional network of pores while formation of connecting channels along a single plane results in planar voids. Planar networks of pores create planes of weakness that can be ruptured under minimal pressure to form platy structure (Brewer, 1976; Figueira and Stoops, 1983; Anderson et al., 2002). The application of HRXCT to study vesicular peds during different stages of vesicular horizon development, both in the lab and in field chronosequence studies, could provide further insights into the genetic pathways of pore development in the vesicular horizon.

Pore Classification Model

The description of observed pores was used to build a classification tree model that applies quantitative metrics of pore shape extracted from a HRXCT scan in Blob3D. The model is designed to create a quantitative system for classification, which is more consistent than classification based on visual observation. Furthermore, with the classification tree model, all of the pores in a sample can be classified in minutes whereas actually observing and describing each individual pore would be an impractical investment of time. To illustrate this point, it took approximately 20 h to examine and describe the 1130 pores used to build and

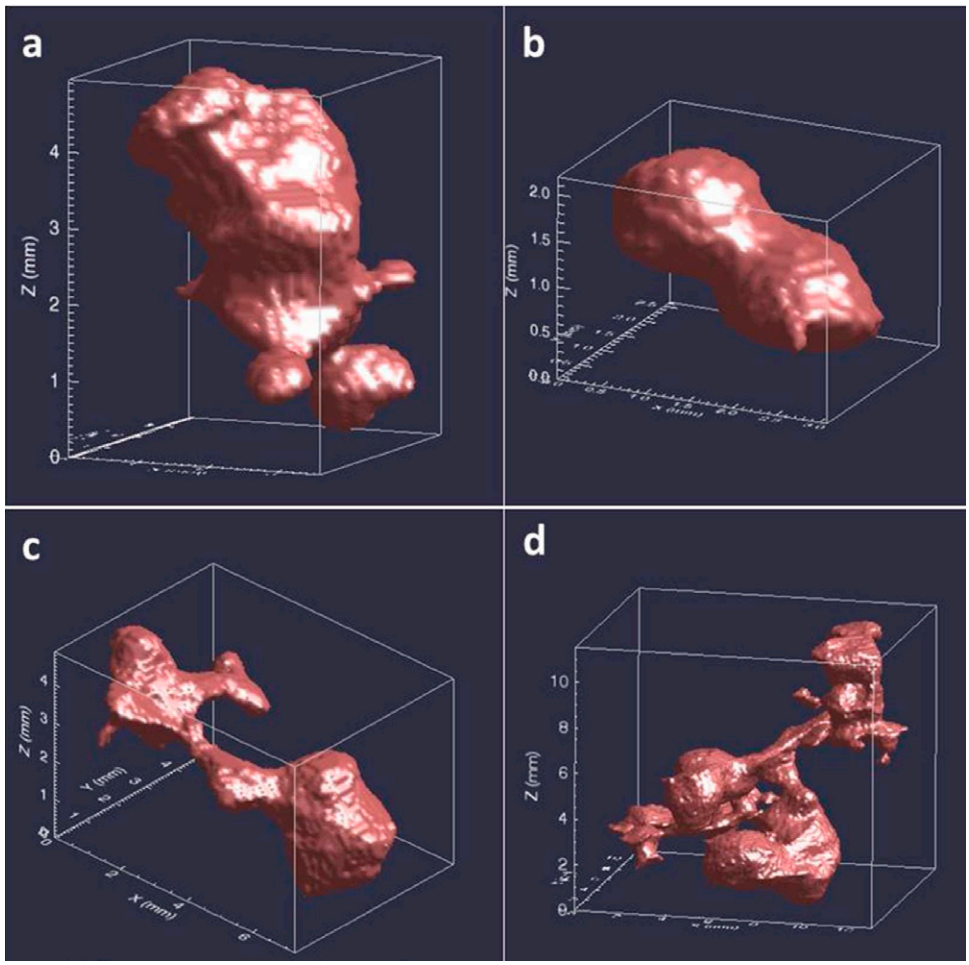

Fig. 4. Images of vughs generated using Blob3D: (a) and (b) examples of isolated vughs and (c) and (d) examples of vughs connected by channels.

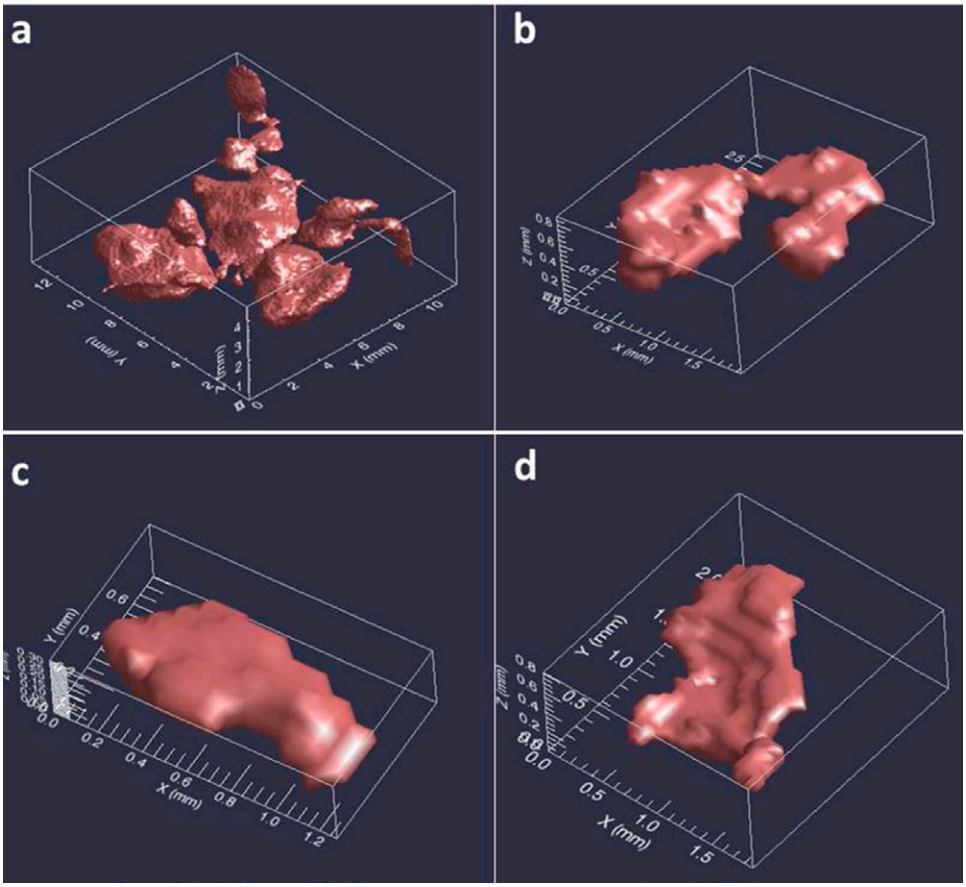

Fig. 5. Images of planar voids using Blob3D: (a) vughs connected along a plane, (b) planar voids connected by a narrow channel, (c) and (d) planar void fragments.

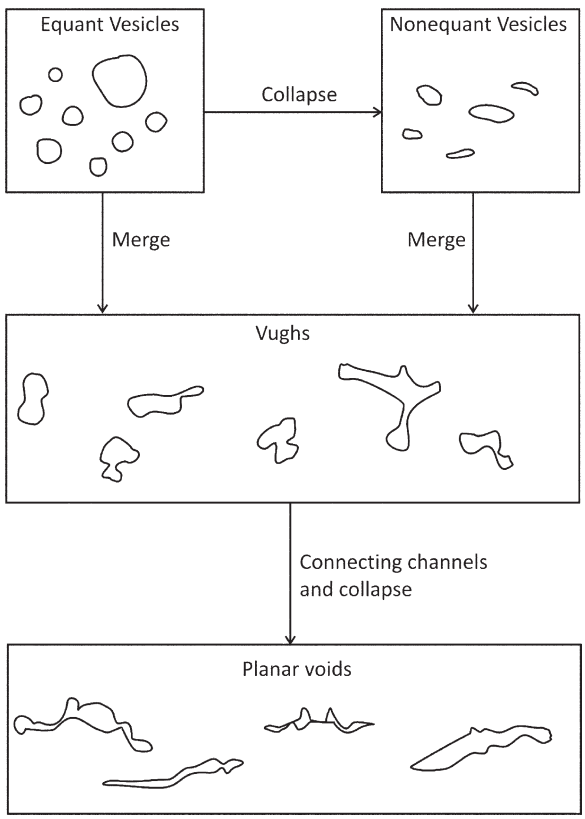

Fig. 6. Proposed genetic pathway for pore development in the vesicular horizon.

test the model, and the entire sample contained 12,300 pores. Previous attempts to use quantitative pore parameters to classify pores have been made (Figueira and Stoops, 1983; Yonovitz and Drohan, 2009); however, these studies have focused primarily on distinguishing vesicles and vughs and were limited to two dimensional parameters measured in thin section. The classification tree model employed here allows the use of more than one model parameter to distinguish a larger array of pore classes.

The classification tree model is illustrated in Fig. 7. The first split that the model makes is between vesicles and other pore types, based on the SNSVR. Vesicles have a lower SNSVR, indicating a more spherical shape. The second split is between equant vesicles and non-equant vesicles (oblate, prolate, and hemispherical) based on AR1. Equant vesicles have a smaller AR1, indicating more equal axis lengths. The model was unable to resolve the difference between oblate, prolate, and hemispherical vesicles, which are treated as a group in all subsequent analyses. The term AR2 was tested as a modeling parameter to help to distinguish the vesicle types but did not show any statistically significant relationships to pore class. The next split in the model is between planar voids and vughs, with planar voids being distinguished by a high AR1, indicating that they are highly elongated in one direction and flattened in another. The last split is then between isolated vughs and interconnected vughs, based on SNSVR. Interconnected vughs were distinguished by a high SNSVR, reflecting their complex shape.

The model was tested using the validation dataset (Table 2). Statistical analysis using the chi-square test indicates a strong association between modeled pore class and observed pores class ($\chi^2 = 465.9$, $P < 0.001$). Agreement between the modeled and observed classification was strong for the equant vesicles, with 78% of the pores classified by the model showing agreement with the observed classification. Slightly weaker agreement was observed for non-equant vesicles (65%) and individual vughs (69%). These lower agreement values reflect difficulty training the model to distinguish between these two pore types due to the correlation between parameters that distinguish the two classes (i.e., as AR1 increases, SNSVR also increases). The model showed the weakest agreement with observed classes for the connected vughs (53%) and planar voids (54%). Many pores described as individual vughs were classified as connected vughs or

planar voids by the model, and many connected vughs were also classified as planar voids by the model. This result stems from the fact that many of the vughs formed by connection of vesicles or smaller vughs along a plane. The model favored the classification of such pores as planar voids while our descriptions favored calling them vughs. This deviation of the model from the observed pore classes is considered acceptable because connected vughs elongated along a plane function like planar voids in that they create planes of weakness and generate localized preferential flow pathways within the vesicular horizon (Anderson et al., 2002).

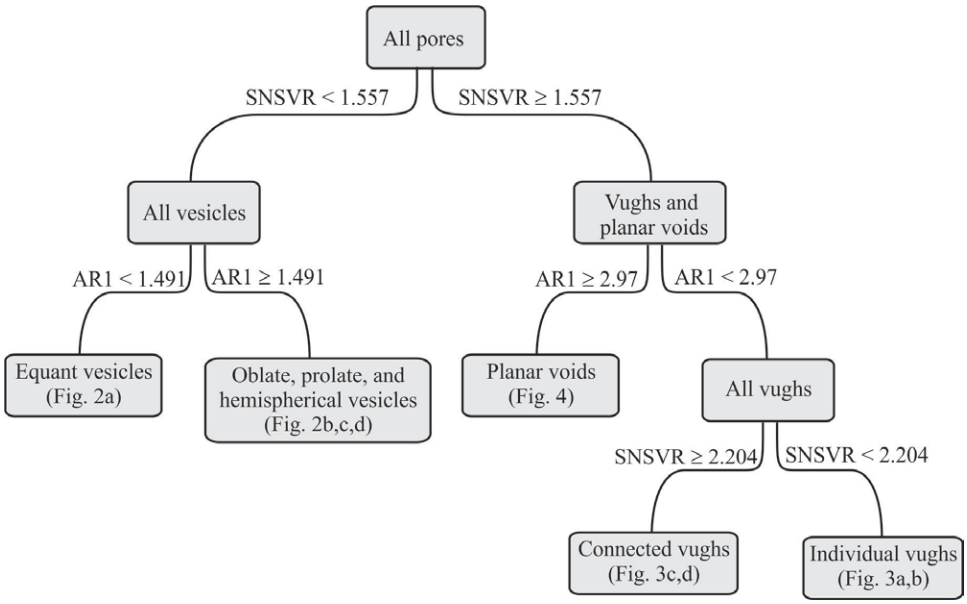

Fig. 7. Classification tree for grouping pores according to shape using parameters extracted from high resolution X-ray computed tomography scan: SNSVR = sphere normalized surface area to volume ration, AR1 = ratio of longest to shortest axis of best fit ellipsoid.

Overall, the model results agreed well with the observed pores class for vesicles, but showed less agreement in vughs and planar void classes. The model shifted the classification of many pores described as vughs towards the planar void class. Though there were some clear deviations, the level of agreement between the model and description results are found to be acceptable. The pore shapes have a degree of continuity that makes drawing an exact line between classes difficult. However, the strong contrast between well-expressed vesicles, vughs, and planar voids necessitates their separation to provide adequate characterization (see Fig. 3, 4, and 5). The classification of pores based on model parameters created a more exact definition of the pore classes. The advantage of the model is its precision and time-saving capacity, though some sacrifice of accuracy is made.

Characterization of Pores

The pores classified according to the model display differences in their size, quantity, and orientation. Connected vughs were significantly larger than all other pore types, although they were the fewest in quantity (Table 3). The large size of the connected vughs reflects their formation through the development of channels between individual vughs, resulting in large networks of pores. These large networks, though few in number, could provide preferential flow pathways within ped interiors, which otherwise restrict water movement (Young et al., 2004; Meadows et al., 2008). The second largest pores were the planar voids and individual vughs. Most planar voids are aligned with their longest axis close to the *x*–*y* plane (Fig. 8b), with variation explained by the alignment of planar voids with the rounded surface of the columnar ped (Fig. 2a). Vughs were larger in size than vesicles (Table 3), lending support to the proposed model of formation through coalescence of vesicles (Fig. 6). Non-equant vesicles were similar in size to the equant vesicles and were the most numerous of all of the pore types (Table 3). The orientation of the longest axis of the non-equant vesicles is most often closely aligned with the *x*–*y* plane of the sample; however, there is more variation in orientation than is seen with the planar voids (Fig.

Table 3. Pore volume and quantity of each pore classes. Averages and standard deviation of the three sites are given. Averages followed by different letters indicate a significant difference between the pore classes at the α = 0.05 level.

Pore class	Pore volume		Pore quantity	
	avg.	SD	avg.	SD
	mm^3		cm^{-3}	
Equant vesicles	0.36a	0.08	20a,b	8
Non-equant vesicles	0.32a	0.14	44a	18
Individual vughs	1.07b	0.33	19a,b	7
Connected vughs	11.0c	4.00	3b	0.7
Planar voids	1.63b	0.45	14b	8

Table 2. Comparison of observed pore class with classification tree model results in the validation dataset.

Classification tree result	Observed pore class					% Agreement
	Equant vesicles	Non-equant vesicles	Individual vughs	Connected vughs	Planar voids	
	No. of pores					
Equant vesicles	57	11	5	0	0	78
Non-equant vesicles	7	55	21	1	0	65
Individual vughs	0	15	61	6	6	69
Connected vughs	0	0	6	8	1	53
Planar voids	0	2	16	14	38	54

8). This suggests that the collapse of equant vesicles to form non-equant vesicles occurs most often along the *z*-axis, presumably due to the weight of the overlying sediment.

Pore Variation with Depth

Analysis of vertical subsections reveals that pore size and quantity vary in relation to depth within the samples. All three peds showed a trend of decreasing number of equant vesicles with increasing depth in the ped (Fig. 9a). Individual vughs and planar voids, however, increased in number with increasing depth in two of the peds (Lida and Tonopah) but showed little change with depth in the ped from Mina (Fig. 9c and 9e). The trend in number of non-equant vesicles and connected vughs with depth, however, showed no similarity between any of the three peds analyzed (Fig. 9b and 9d). All pore types showed a trend of decreasing volume with increasing depth, across nearly all samples, the exception being equant vesicles and planar voids in the Tonopah sample (Fig. 10). Other authors have observed the vesicles near the surface are larger and more equant (Hugie and Passey, 1964; Bouza et al., 1993), and some have divided the vesicular horizon into two morphological zones, with the surface zone being dominated by vesicles and the lower portion dominated by platy structure (Lebedeva et al., 2009; Dietze et al., 2012). However, previous quantitative studies using two-dimensional characterization have failed to find evidence of a trend in pore size and shape with depth (Dietze et al., 2012). The classification method and three-dimensional HRXCT imagery used in this study make it possible to quantify changes in pore morphology with depth in the vesicular horizon.

Possible reasons for the changes in pore morphology with depth include increased overburden weight with depth, decreased frequency of wetting with depth, and more recent deposition of eolian sediment near the surface of the vesicular horizon. The decrease in size of all pore classes may be attributed to the influence of overburden weight and frequency of wetting. Near the surface, there is less overburden weight, which allows pores to grow to a larger size without collapsing. Furthermore, vesicular pores are known to grow in size as the soil is exposed to wetting and drying cycles (Miller, 1971; Figueira and Stoops, 1983). Thus, small rainstorms that only wet the surface of the soil may promote growth of pores near the surface while pores deeper in the soil only experience periods of growth during large rainstorms. Some authors have suggested a relation of pore size with depth to the thermal gradient of the soil and greater heating of the soil surface (Bouza et al., 1993); however, subsequent experimental work has shown that there is no effect of heating on the size of vesicular pores (Dietze et al., 2012; Turk, 2012). The change in relative abundance of equant vesicles compared to other pore types may relate to the age of the sediment due to the accumulation of recent eolian sediments above older sediments in the vesicular horizons. The surface of the vesicular horizon may be considered to be in an earlier stage of development, in which vesicles have undergone less collapse, coalescence, and development of interconnecting channels.

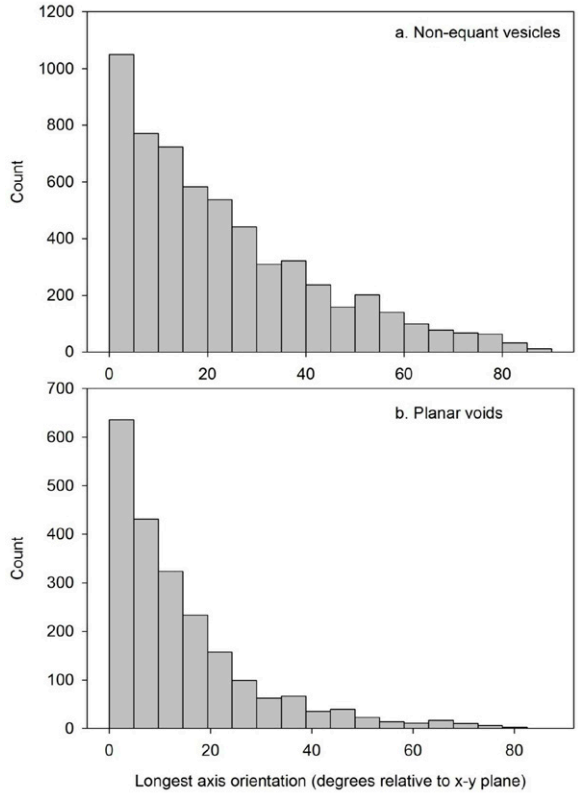

Fig. 8. Histograms of largest axis orientation relative to the x–y plane for: (a) non-equant vesicles and (b) planar voids in the sample from Lida, NV.

Differences between the peds may be attributable to changes in vesicular horizon with increasing age and development. There is an increase in soil age and development between the Lida, Tonopah, and Mina soils (Table 1). In comparing the younger soil (Lida) with the oldest soil (Mina), all pore types increase in size, but decrease in number. The difference in pore morphology with soil age may be related to alteration of the pore morphology over a greater number of wetting and drying cycles (Miller, 1971) and a longer history of eolian accumulation, creating a soil that is more conducive to vesicle growth (Yonovitz and Drohan, 2009).

Pore Variation between Ped Interior and Exterior

The peds collected from Lida and Tonopah showed a trend of decreasing number of pores, across all pores types, with increasing distance from the ped center (Fig. 11). At Mina, this trend was observed, but to a lesser degree, for equant vesicles, non-equant vesicles, and individual vughs and was not observed for connected vughs and planar voids. At Lida, there was also an increase in pores size with increasing distance from the ped center, a trend that was not observed in the samples from Tonopah and Mina, which had larger pores overall (Fig. 12).

These trends can most likely be attributed to more frequent wetting of the ped exterior. Preferential flow between columnar peds has been observed to occur in the vesicular horizon (Meadows et al., 2008). Thus, the exterior of the peds become wet first, while the ped interior only becomes wet during large rainstorms. Laboratory experiments have demonstrated that with an increasing number of wetting cycles, vesicular pores and vughs in-

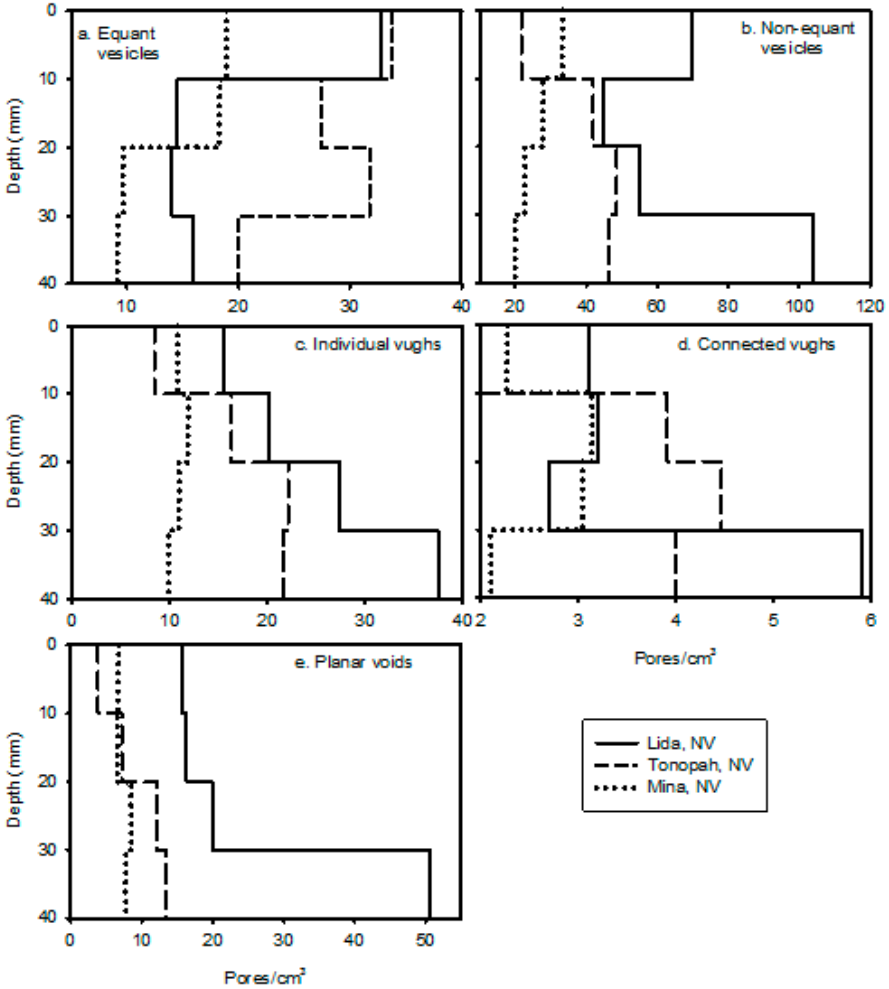

Fig. 9. Number of pores per sample volume at different depth ranges within the ped for each pore class: (a) equant vesicles, (b) non-equant vesicles, (c) individual vughs, (d) connected vughs, (e) planar voids.

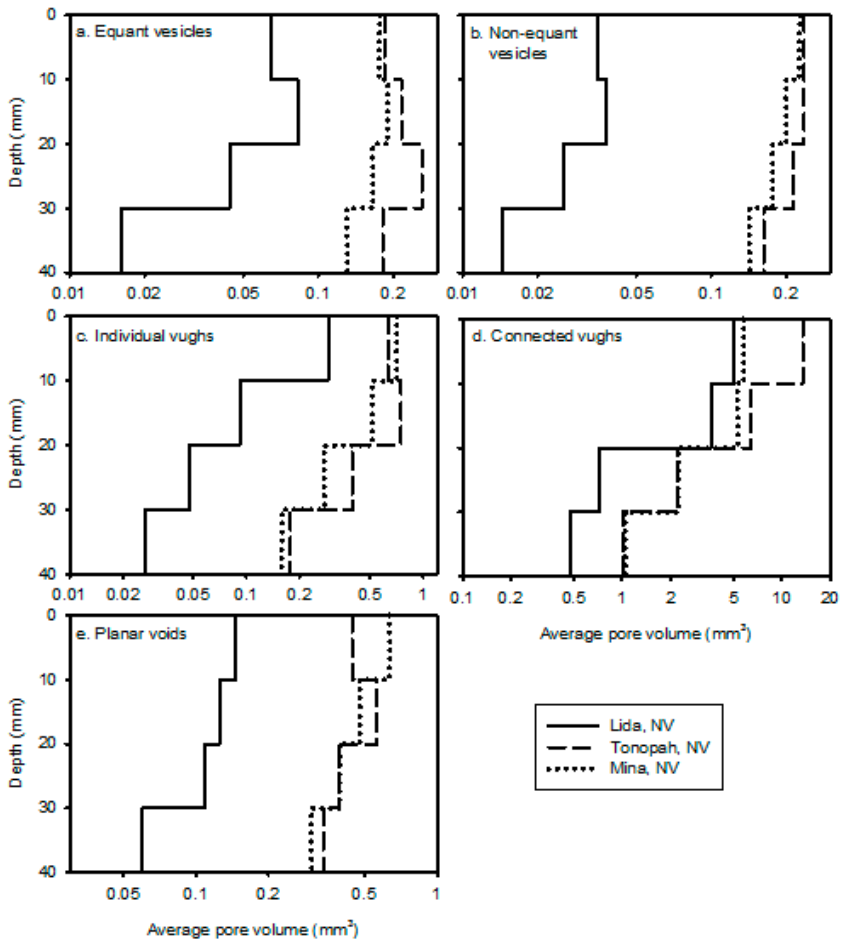

Fig. 10. Average pore volume at different depth ranges within the ped for each pore class: (a) equant vesicles, (b) non-equant vesicles, (c) individual vughs, (d) connected vughs, (e) planar voids.

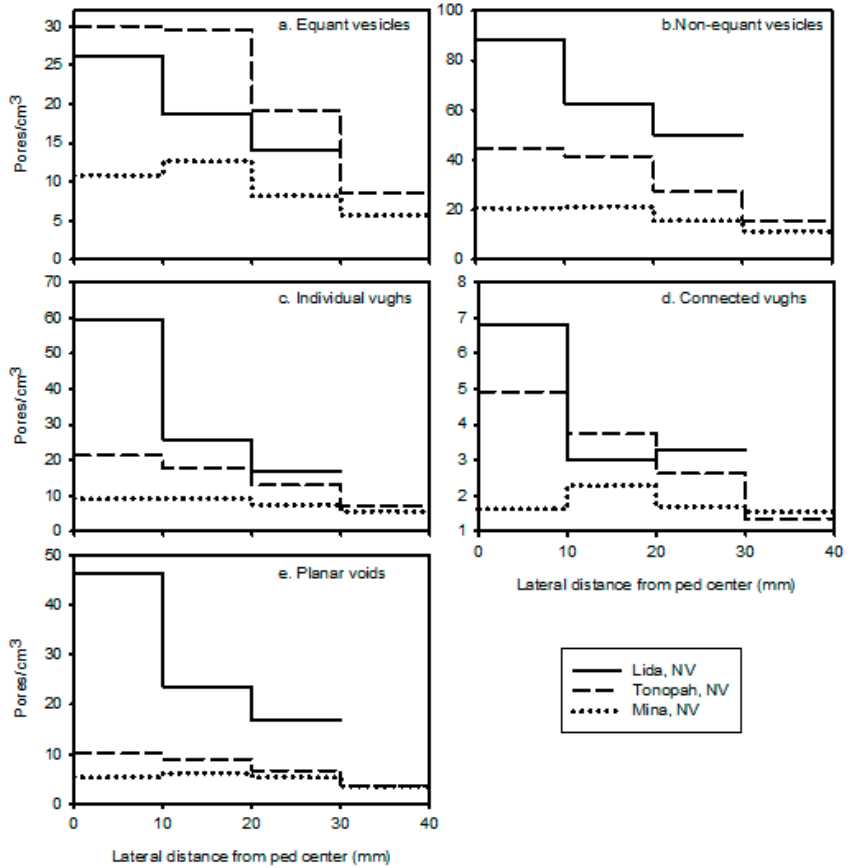

Fig. 11. Number of pores per sample volume at lateral distances from the ped center for each pore class: (a) equant vesicles, (b) non-equant vesicles, (c) individual vughs, (d) connected vughs, (e) planar voids.

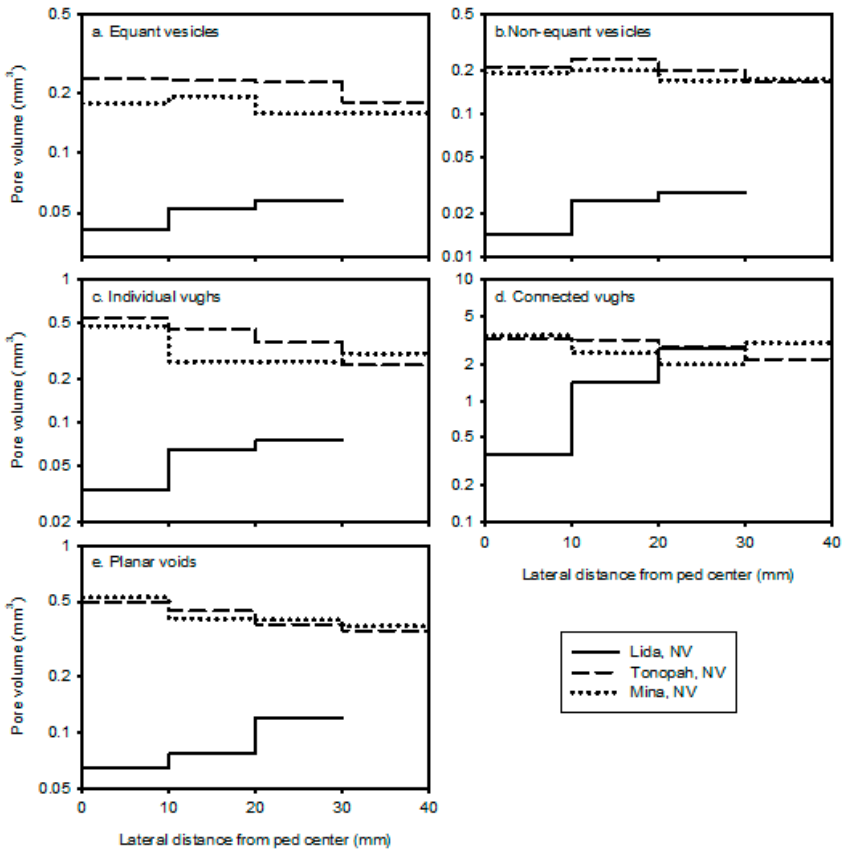

Fig. 12. Average pore volume at different lateral distances from the ped center for each pore class: (a) equant vesicles, (b) non-equant vesicles, (c) individual vughs, (d) connected vughs, (e) planar voids.

crease in size and decrease in number due to growth and merging of adjacent pores (Figueira and Stoops, 1983). This may explain why the exterior of the ped, which is wet more frequently, has larger but less numerous pores. There was less difference between the ped interior and exterior in the samples from Mina, reflecting a more advanced stage of vesicular horizon development.

SUMMARY AND CONCLUSIONS

In this study, five classes of pores occurring within the vesicular horizon have been described. Methods were developed to classify of the pores using quantitative data extracted from HRXCT scans (Fig. 7). The pore classes are equant vesicles, non-equant vesicles, individual vughs, connected vughs, and planar voids. The most likely genetic relationship between these pore types involves the collapse, coalescence, and development of channels between pores. The connected vughs, though few in number, were the largest pores contained within the sample, with potential significance with regards to intrapedal movement of water. Significant changes in pore size and quantity were observed with depth and lateral distance from the center of the ped. The variability in pore characteristics in different parts of the same ped suggests that whole ped characterization is required to get the complete picture of pore morphology within the vesicular horizon.

The methods of pore classification and characterization introduced and evaluated here may be effectively applied in the study of vesicular horizons and soils displaying similar pore types. Such applications include understanding the relationship between vesicular pore morphology and climate regime (Turk and Graham, 2011), studying the effects of disturbance on vesicular pore morphology (Yonovitz and Drohan, 2009), developing methods to relate vesicular pore shape to historical dust deposition rates (Dietze et al., 2012), understanding the hydrology of vesicular horizons (Young et al., 2004, Meadows et al., 2005, Meadows et al., 2008), and characterizing porosity in fragipan soils (Pelton et al., 2013).

ACKNOWLEDGMENTS

Funded by contract 68-7482-9-542 with USDA-NRCS and NSF award 1110425. Computed tomography scanning was performed by the University of Texas High-Resolution X-Ray Computed Tomography Facility.

REFERENCES

Abrahams, A.D., and A.J. Parsons. 1991. Relation between infiltration and stone cover on a semiarid hillslope, southern Arizona. J. Hydrol. 122:49–59. doi:10.1016/0022-1694(91)90171-D

Amit, R., and R. Gerson. 1986. The evolution of Holocene reg (gravelly) soils in deserts: An example from the Dead Sea region. Catena 13:59–79. doi:10.1016/S0341-8162(86)80005-4

Anderson, K., S. Wells, and R. Graham. 2002. Pedogenesis of vesicular horizons, Cima Volcanic Field, Mojave Desert, California. Soil Sci. Soc. Am. J. 66:878–887. doi:10.2136/sssaj2002.0878

Badorreck, A., H.H. Gerke, and R.F. Hüttl. 2013. Morphology of physical soil crusts and infiltration patterns in an artificial catchment. Soil Tillage Res. 129:1–8. doi:10.1016/j.still.2013.01.001

Bell, J.W. 1995. Quaternary geologic map of the Mina quadrangle, NV. Nevada Bureau of Mines and Geology, Reno, NV.

Blackburn, W.H. 1975. Factors influencing infiltration and sediment production of semiarid rangelands in Nevada. Water Resour. Res. 11:929–937. doi:10.1029/WR011i006p00929

Bouza, P., H.F. Delvalle, and P.A. Imbellone. 1993. Micromorphological, physical, and chemical characteristics of soil crust types of the central Patagonia region, Argentina. Arid Soil Res. Rehabil. 7:355–368. doi:10.1080/15324989309381368

Brewer, R. 1976. Fabric and mineral analysis of soils. Krieger, Huntington, NY.

Brown, K.J., and D.L. Dunkerley. 1996. The influence of hillslope gradient, regolith texture, stone size and stone position on the presence of a vesicular layer and related aspects of hillslope hydrologic processes: A case study from the Australian arid zone. Catena 26:71–84. doi:10.1016/0341-8162(95)00034-8

Brun, F., L. Mancini, P. Kasae, S. Favretto, D. Dreossi, and G. Tromba. 2010. Pore3D: A software library for quantitative analysis of porous media. Nucl. Instrum. Methods Phys. Res. A 615:326–332. doi:10.1016/j.nima.2010.02.063

Cantón, Y., A. Solé-Benet, and R. Lázaro. 2003. Soil-geomorphology relations in gypsiferous materials of the Tabernas Desert (Almeria, SE Spain). Geoderma 115:193–222.

Clements, T., R.H. Merriam, R.O. Stone, J.L. Eymann, and H.L. Reade. 1957. A study of desert surface conditions. EP-53. Environmental Protection Research Division, Natick, MA.

Dan, J., D.H. Yaalon, R. Moshe, and S. Nissim. 1982. Evolution of reg soils in southern Israel and Sinai. Geoderma 28:173–202. doi:10.1016/0016-7061(82)90002-7

Dietze, M., S. Bartel, M. Lindner, and A. Kleber. 2012. Formation mechanisms and control factors of vesicular soil structure. Catena 99:83–96. doi:10.1016/j.catena.2012.06.011

Ellis, F. 1990. Note on soils with vesicular structure and other micromorphological features in Karoo soils. Congr. Soil Sci. Soc. S. Afr., Pretoria. 16:326–336.

Eshel, G., G.J. Levy, U. Mingelgrin, and M.J. Singer. 2004. Critical evaluation of the use of laser diffraction for particle-size distribution analysis. Soil Sci. Soc. Am. J. 68:736–743. doi:10.2136/sssaj2004.7360

Evenari, M., D.H. Yaalon, and Y. Gutterman. 1974. Note on soils with vesicular structure in deserts. Z. Geomorphol. 18:162–172.

Figueira, H., and G. Stoops. 1983. Application of micromorphometric techniques to the experimental study of vesicular layer formation. Pedologie 33:77–89.

Henning, J.A.G., and K. Kellner. 1994. Degradation of a soil (Aridosol) and vegetation in the semiarid grasslands of southern Africa. Bot. Bull. Acad. Sin. 35:195–199.

Hillel, D. 1998. Environmental soil physics. Academic Press, San Diego, CA.

Hothorn, T., K. Hornik, and A. Zeileis. 2006. Unbiased recursive partitioning: A conditional inference framework. J. Comput. Graph. Statist. 15:651–674. doi:10.1198/106186006X133933

Hugie, V.K., and H.B. Passey. 1964. Soil surface patterns of some semiarid soils in northern Utah, southern Idaho, and northeastern Nevada. Soil Sci. Soc. Am. Proc. 28:786–792. doi:10.2136/sssaj1964.03615995002800060030x

Jerram, D.A., A. Mock, G.R. Davis, M. Field, and R.J. Brown. 2009. 3D crystal size distributions: A case study on quantifying olivine populations in kimberlites. Lithos 112:223–235. doi:10.1016/j.lithos.2009.05.042

Joeckel, R.M., and B.A. Clement. 1999. Surface features of the Salt Basin of Lancaster County, Nebraska. Catena 34:243–275. doi:10.1016/S0341-8162(98)00114-3

Ketcham, R.A. 2005. Computational methods for quantitative analysis of three-dimensional feature in geological specimens. Geosphere 1:32–41. doi:10.1130/GES00001.1

Ketcham, R.A., and W.D. Carlson. 2001. Acquisition, optimization and interpretation of X-ray computed tomographic imagery: Applications to the geosciences. Comput. Geosci. 27:381–400. doi:10.1016/S0098-3004(00)00116-3

Lebedeva, M.P., D.L. Golovanov, and S.A. Inozemtsev. 2009. Microfabrics of desert soils of Mongolia. Euras. Soil Sci. 42:1204–1217.

Malam Issa, O.M., J. Trichet, C. Defarge, A. Coute, and C. Valentin. 1999. Morphology and microstructure of microbiotic soil crusts on a tiger bush sequence (Niger, Sahel). Catena 37:175–196. doi:10.1016/S0341-8162(99)00052-1

McAuliffe, J.R. 1994. Landscape evolution, soil formation, and ecological patterns and processes in Sonoran Desert bajadas. Ecol. Monogr. 64:111–148. doi:10.2307/2937038

McFadden, L.D., E.V. McDonald, S.G. Wells, K. Anderson, J. Quade, and S.L. Forman. 1998. The vesicular layer and carbonate collars of desert soils and pavements: Formation, age and relation to climate change. Geomorphology 24:101–145. doi:10.1016/S0169-555X(97)00095-0

McFadden, L.D., S.G. Wells, and M.J. Jercinovich. 1987. Influences of eolian and pedogenic processes on the origin and evolution of desert pavements. Geology 15:504–508. doi:10.1130/0091-7613(1987)15<504:IOEAPP>2.0.CO;2

Meadows, D.G., M.H. Young, and E.V. McDonald. 2005. A laboratory method for determining the unsaturated hydraulic properties of soil peds. Soil Sci. Soc. Am. J. 69:807–815. doi:10.2136/sssaj2004.0191

Meadows, D.G., M.H. Young, and E.V. McDonald. 2008. Influence of relative surface age on hydraulic properties and infiltration on soils associated with desert pavements. Catena 72:169–178. doi:10.1016/j.catena.2007.05.009

Miller, D.E. 1971. Formation of vesicular structure in Soil. Soil Sci. Soc. Am. Proc. 35:635–637. doi:10.2136/sssaj1971.03615995003500040042x

Musick, H.B. 1975. Barrenness of desert pavement in Yuma County, Arizona. J. Arizona Acad. Sci. 10:24–28.

Noy-Meir, I. 1973. Desert ecosystems: Environment and producers. Annu. Rev. Ecol. Syst. 4:25–51. doi:10.1146/annurev.es.04.110173.000325

Paletskaya, L.N., A.P. Lavrov, and S.I. Kogan. 1958. Pore formation in takyr crust. Sov. Soil Sci. (Engl. Transl.) 3:245–250.

Pelton, G., B.D. Lee, and J.K. Turk. 2013. Pore space and concretion distribution in a prairie mound fragipan. Poster session presented at: Water, Food, Energy, and Innovation for a sustainable world. ASA, SSSA, CSSA International Annual Meetings. Tampa, FL. 3–6 Nov. Poster 1703.

Peterson, F.F. 1981. Landforms of the Basin and Range Province: Defined for soil survey. Nevada Agric. Exp. Stn. Tech. Bull. 28. University of Nevada, Reno.

Segal, E., P.J. Shouse, S.A. Bradford, T.H. Skaggs, and D.L. Corwin. 2009. Measuring particle size distribution using laser diffraction: Implications for predicting soil hydraulic properties. Soil Sci. 174:639–645. doi:10.1097/SS.0b013e3181c2a928

Shafer, D.S., M.H. Young, S.F. Zitzer, T.G. Caldwell, and E.V. McDonald. 2007. Impacts of interrelated biotic and abiotic processes during the past 125,000 years of landscape evolution in the Northern Mojave Desert, Nevada, USA. J. Arid Environ. 69:633–657. doi:10.1016/j.jaridenv.2006.11.011

Soil Survey Staff. 2010. Keys to Soil Taxonomy. 11th ed. USDA Natural Resources Conservation Service, Washington, DC.

Stoops, G. 2003. Guidelines for analysis and description of soil and regolith thin sections. Soil Science Society of America., Madison, WI.

Sullivan, L.A., and A.J. Koppi. 1991. Morphology and genesis of silt and clay coatings in the vesicular layer of a desert loam soil. Aust. J. Soil Res. 29:579–586. doi:10.1071/SR9910579

Turk, J.K. 2012. Vesicular horizon distribution, properties, and pedogenic processes in deserts of the western United States. Ph.D. diss., Univ. of California, Riverside.

Turk, J.K., and R.C. Graham. 2011. Distribution and properties of vesicular horizons in the western United States. Soil Sci. Soc. Am. J. 75:1449–1461. doi:10.2136/sssaj2010.0445

Ugolini, F.C., S. Hillier, G. Certini, and M.J. Wilson. 2008. The contribution of aeolian material to an Aridisol from southern Jordan as revealed by mineralogical analysis. J. Arid Environ. 72:1431–1447. doi:10.1016/j.jaridenv.2008.02.014

USGS. 2009. Global land survey 2000. Landsat ETM+. Mosaic N-11–35. USGS, Sioux Falls, SD.

Valentin, C. 1994. Surface sealing as affected by various rock fragment covers in West-Africa. Catena 23:87–97. doi:10.1016/0341-8162(94)90055-8

Valentine, G.A., and C.D. Harrington. 2006. Clast size controls and longevity of Pleistocene desert pavements at Lathrop Wells and Red Cone volcanoes, southern Nevada. Geology 34:533–536. doi:10.1130/G22481.1

Wells, S.G., L.D. McFadden, J. Poths, and C.T. Olinger. 1995. Cosmogenic ^{3}He surface-exposure dating of stone pavements: Implications for landscape evolution in deserts. Geology 23:613–616. doi:10.1130/0091-7613(1995)023<0613:CHSEDO>2.3.CO;2

Williams, A.J., B.J. Buck, and M.A. Beyene. 2012. Biological soil crusts in the Mojave Desert: Micromorphology and pedogenesis. Soil Sci. Soc. Am. J. 76:1685–1695.

Wood, M.K., W.H. Blackburn, R.E. Eckert, and F.F. Peterson. 1978. Interrelations of physical-properties of coppice dune and vesicular dune interspace soils with grass seedling emergence. J. Range Manage. 31:189–192. doi:10.2307/3897177

Wood, Y.A., R.C. Graham, and S.G. Wells. 2005. Surface control of desert pavement pedologic process and landscape function, Cima Volcanic field, Mojave Desert, California. Catena 59:205–230. doi:10.1016/j.catena.2004.06.001

Yonovitz, M., and P.J. Drohan. 2009. Pore morphology characteristics of vesicular horizons in undisturbed and disturbed arid soils; implications for arid land management. Soil Use Manage. 25:293–302. doi:10.1111/j.1475-2743.2009.00225.x

Young, M.H., E.V. McDonald, T.G. Caldwell, S.G. Benner, and D.G. Meadows. 2004. Hydraulic properties of a desert soil chronosequence in the Mojave Desert, USA. Vadose Zone J. 3:956–963. doi:10.2113/3.3.956